European Journal of Radiology Open 11 (2023) 100516

Contents lists available at ScienceDirect

European Journal of Radiology Open

journal homepage: www.elsevier.com/locate/ejro

Reproducibility of quantitative ADC, T1, and T2 measurement on the cerebral cortex: Utility of whole brain echo-planar DWI with compressed SENSE (EPICS-DWI): A pilot study

Koji Yamashita [a,*], Masami Yoneyama [b], Kazufumi Kikuchi [c], Tatsuhiro Wada [d], Hiroo Murazaki [d], Hiroaki Watanuki [d], Ryoji Mikayama [d], Kousei Ishigami [c], Osamu Togao [e]

[a] Departments of Radiology Informatics and Network, Graduate School of Medical Sciences, Kyushu University, 3-1-1, Maidashi, Higashi-ku, Fukuoka 812-8582, Japan
[b] Philips Japan, 13-37, Kohnan 2-chome, Minato-ku, Tokyo 108-8507, Japan
[c] Departments of Clinical Radiology, and Graduate School of Medical Sciences, Kyushu University, 3-1-1, Maidashi, Higashi-ku, Fukuoka 812-8582, Japan
[d] Division of Radiology, Department of Medical Technology, Kyushu University Hospital, Japan
[e] Departments of Molecular Imaging and Diagnosis, Graduate School of Medical Sciences, Kyushu University, 3-1-1, Maidashi, Higashi-ku, Fukuoka 812-8582, Japan

HIGHLIGHTS

- In this pilot study, the ICCs for ADC, T1, T2, and PD were 0.785, 0.986, 0.978, and 0.968, indicating high reproducibility.
- Cerebral cortices showed relatively high ADC, T1, T2, and PD in the mean than white matter regions and subcortical nuclei.
- Combination of EPICS-DWI and 3D-QALAS displayed the high reproducibility of ADC, T1, T2, and PD for cerebral cortices.

ARTICLE INFO

Keywords:
Magnetic resonance imaging
Diffusion magnetic resonance imaging
Brain
Cerebral cortex
Test retest reliability

ABSTRACT

Purpose: To assess the reproducibility of ADC, T1, T2, and proton density (PD) measurements on the cortex across the entire brain using high-resolution pseudo-3D diffusion-weighted imaging using echo-planar imaging with compressed SENSE (EPICS-DWI) and 3D quantification with an interleaved Look-Locker acquisition sequence with T2 preparation pulse (3D-QALAS) in normal healthy adults.

Methods: Twelve healthy participants (median age, 33 years; range, 28–51 years) were recruited to evaluate the reproducibility of whole-brain EPICS-DWI and synthetic MRI. EPICS-DWI utilizes a compressed SENSE reconstruction framework while maintaining the EPI sampling pattern. The 3D-QALAS sequence is based on multi-acquisition 3D gradient echo, with five acquisitions equally spaced in time, interleaved with a T2 preparation pulse and an inversion pulse. EPICS-DWI (*b* values, 0 and 1000 s/mm^2) and 3D-QALAS sequence with identical voxel size on a 3.0-T MR system were performed twice (for test-retest scan). Intraclass correlation coefficients (ICCs) for ADC, T1, T2, and PD for all parcellated volume of interest (VOI) per subject on scan-rescan tests were calculated to assess reproducibility. Bland-Altman plots were used to investigate discrepancies in ADCs, T1s, T2s, and PDs obtained from the two MR scans.

Results: The ICC of ADCs was 0.785, indicating "good" reproducibility. The ICCs of T1s, T2s, and PDs were 0.986, 0.978, and 0.968, indicating "excellent" reproducibility.

Conclusion: The combination of EPICS-DWI and 3D-QALAS sequences with identical voxel size could reproducible ADC, T1, T2, and PD measurements for the cortex across the entire brain in healthy adults.

Abbreviations: 3D-QALAS, 3D quantification with an interleaved Look-Locker acquisition sequence with T2 preparation pulse; ADC, apparent diffusion coefficient; EPICS-DWI, DWI using echo planar imaging with compressed SENSE; FOV, field of view; ICC, Intraclass correlation coefficients; PD, proton density; SENSE, sensitivity encoding; VOI, volume of interest.

* Corresponding author.
E-mail address: yamashita.koji.659@m.kyushu-u.ac.jp (K. Yamashita).

https://doi.org/10.1016/j.ejro.2023.100516
Received 24 April 2023; Received in revised form 30 July 2023; Accepted 8 August 2023
Available online 11 August 2023

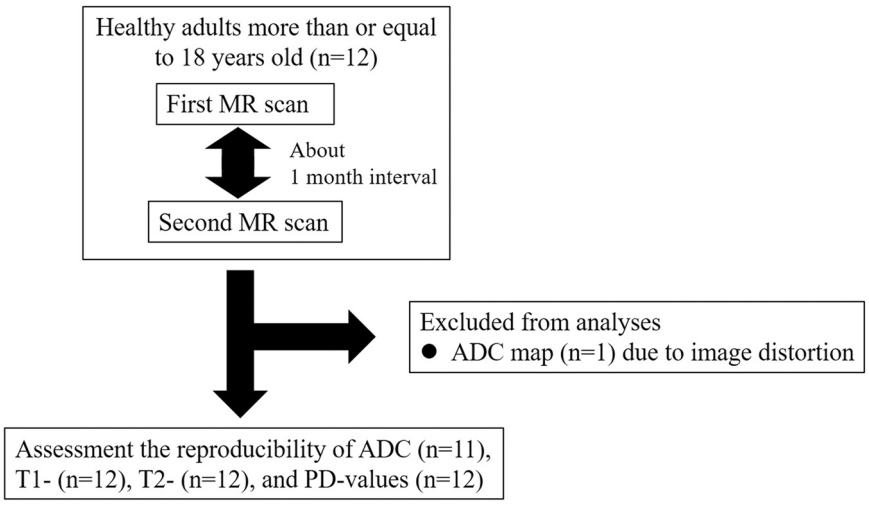

Fig. 1. Flow diagram of participation in the present study.

1. Introduction

MR imaging is widely used for investigating degenerative diseases, developmental processes, and so on. Of these, diffusion-weighted imaging (DWI) plays a pivotal role in non-invasively measuring the incoherent Brownian motion of water molecules in biological tissues [1]. The apparent diffusion coefficient (ADC) is known to correlate with neuronal loss and astrogliosis in the cerebral cortex, as well as axonal degeneration, demyelination, and gliosis in white matter [2,3]. However, conventional 2D DWI provides unreliable ADCs mainly due to the partial volume effect. High-resolution DWI might reduce the partial volume effect, while it demands long scan time when targeting the whole brain [4]. Another drawback of high-resolution DWI would be geometry factor-induced noise or band-like artifacts [5,6], which limits the accuracy of ADCs [7]. Recently, pseudo-3D DWI using echo planar imaging with compressed SENSE (EPICS-DWI) was proposed [5]. EPICS-DWI minimizes these band-like artifacts and accordingly improves image resolution and quality without prolonging scan time [5,6,8].

In terms of predicting microscopic white matter change, T1, T2, and proton density (PD) measurements have been utilized to estimate cortical myelin. Hyperintensity on T1-weighted imaging and hypointensity on T2-weighted imaging are known to be associated with myelin-bound cholesterol [9] and myelin content [9,10], respectively. Calculating the ratio of T1-weighted images to T2-weighted images (T1w/T2w) is one practical approach to estimating myelin content. The ratio of T1w/T2w measurement is reportedly suitable as a surrogate marker for clinical myelin mapping [9,11,12]. However, the evidence from histology is limited and the ratio of T1w/T2w may not be suitable to predict myelin content [13]. 3D quantification with an interleaved Look-Locker acquisition sequence with T2 preparation pulse (3D-QALAS) sequence have allowed simultaneous tissue relaxometry of T1 and T2 relaxation times and PD [14,15]. The 3D-QALAS sequence enables not only 3D acquisition of the whole brain in high resolution but

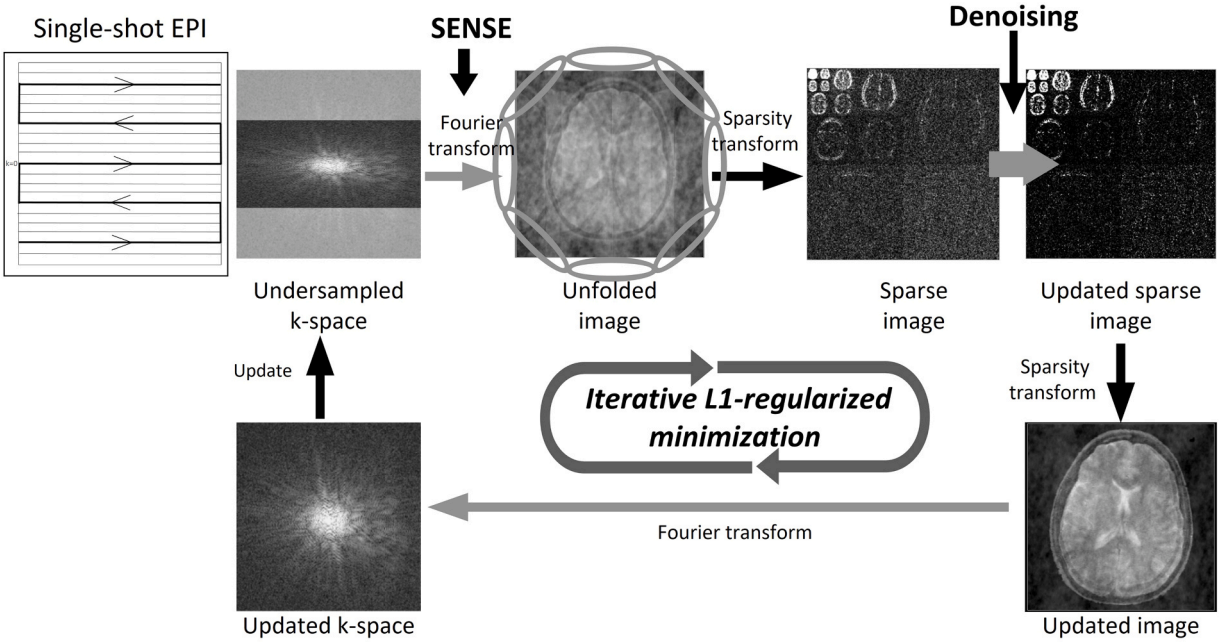

Fig. 2. Schematic illustration of EPI with Compressed SENSE (EPICS). In the EPICS framework, the EPI sampling pattern provides equispaced regular undersampling, similar to SENSE-EPI. For reconstruction, wavelet-based iterative L1-regularized minimization is integrated with SENSE unfolding to achieve an optimal balance between noise and data consistency.

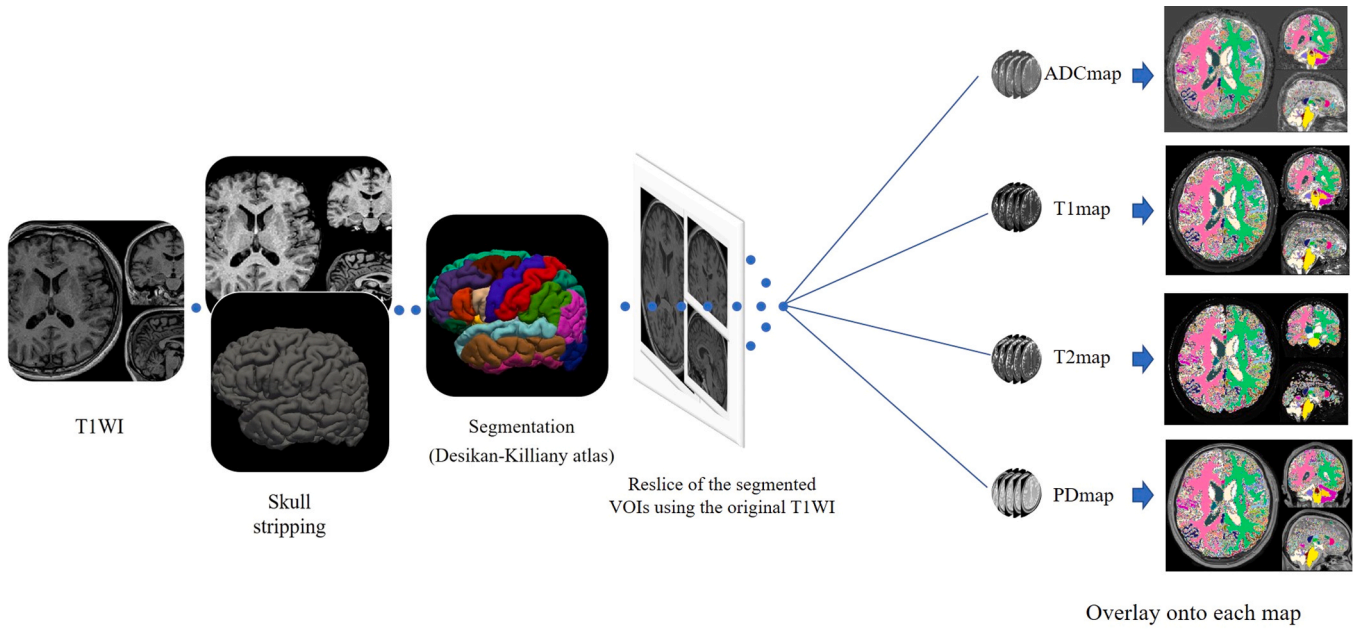

Fig. 3. The implementation flow chart of post-processing techniques. T1-weighed images are resliced to a 1-mm isovoxel space with the FreeSurfer pipeline (https://surfer.nmr.mgh.harvard.edu/fswiki/recon-all). Automatic reconstruction steps include skull stripping and cortical parcellation using the Desikan-Killiany cortical atlas. The acquired Desikan-Killiany atlas of each subject is resliced with the original T1-weighted images. Subsequently, the resliced segmentation atlas is overlaid onto the corresponding ADC, T1, T2, and PD maps using ITK-SNAP software (version 3.8.0; https://dss.itksnap.org) to compute ADC, T1, T2, and PD.

also post-acquisition synthesis of multiple contrast-weighted images from a single 3D scan.

We therefore hypothesized that the combination of quantifiable ADC, T1, T2, and PD with the identical voxel size could help characterize the biological properties of brain tissues, while the reproducibility of measurements of these parameters remains unclear. Our purpose in this study was to assess the reproducibility of ADC, T1, T2, and PD measurements on the cortex across the entire brain using pseudo-3D EPICS-DWI and 3D-QALAS with the identical voxel size in healthy adults.

2. Materials and methods

This prospective study was performed with the approval of the Kyushu University Institutional Review Board for Clinical Trial. Written informed consent was obtained from all participants prior to enrollment. All subjects fulfill the following criterion: healthy adults equal or more than 18 years old; exclusion criteria are: they had implantable cardiac devices, had claustrophobia, or if MR images were degraded or distorted. A flow diagram of participation is shown in Fig. 1. Twelve healthy participants (median age, 33 years; range, 28–51 years; 9 males, 3 females) were recruited to evaluate the reproducibility of whole-brain EPICS-DWI and synthetic MRI. The Mini-Mental State Examination (MMSE) was implemented prior to MRI as a screening tool to evaluate cognitive function.

All MRI was performed using at a 3.0-T scanner (Ingenia Elition X, Philips Healthcare, Best, The Netherlands) equipped with a 20-channel head/neck coil. EPICS-DWI utilizes a compressed SENSE (a combined compressed sensing and parallel imaging technique) reconstruction framework while maintaining the EPI sampling pattern (Fig. 2). Compressed SENSE is an integrated iterative reconstruction loop. In this reconstruction loop, SENSE unfolding is applied iteratively as well as the wavelet-based L1-minimization. After the iterative SENSE unfolding, only non-uniformly distributed g-factor and coil geometry-related noise remains, then wavelet denoising reduces such noise effectively. Consequently, EPICS-DWI minimizes band-like artifacts compared to conventional SENSE-DWI [5,6,8]. Scan parameters for EPICS-DWI in this study were as follows: axial acquisition; repetition time (TR), 20,000 ms; echo time (TE), 58 ms; field-of-view (FOV), 256 × 256 mm^2; matrix size, 224 × 217 (reconstruction matrix, 512 ×512); compressed sensing-SENSE factor, 3.8; *b* values, 0 and 1000 s/mm^2; slice thickness, 1.15 mm; flip angle, 90°; number of averages, 2; acquisition time, 5 min 40 s

The 3D-QALAS sequence is based on multi-acquisition 3D gradient echo, with five acquisitions equally spaced in time, interleaved with a T2 preparation pulse and an inversion pulse [16]. Scan parameters for 3D-QALAS in this study were as follows: axial acquisition; TR, 4.9 ms; TE, 2.2 ms; inversion delay times, 100, 1000, 1900, and 2800 ms; T2-prep echo time, 100 ms; FOV, 256 × 256 mm^2; matrix size, 224 × 217 (reconstruction matrix, 512 ×512); section thickness, 1.15 mm; flip angle, 4°; receiver bandwidth, 393 Hz/pixel; number of averages, 3; acquisition time, 9 min 51 s. Images obtained from the 3D-QALAS sequence were preprocessed on prototype SyMRI software (version 0.45.34; SyntheticMR, Linköping, Sweden) to obtain T1-weighted images, T1 maps, T2 maps, and PD maps.

All subjects took part in two sessions. In each session, EPICS-DWI and 3D-QALAS sequences were acquired from each subject. The interval of the two sessions ranged from 0 to 39 days (median, 22 days). Three participants were administered test-retest scan on the same day. In such cases, the second scan was performed following a 5-min break. ADC maps were calculated from a pair of DWI (*b* factors, 0 and 1000 s/mm^2). T1 maps, T2 maps, and PD maps were generated using SyMRI software for volume of interest (VOI) analysis.

2.1. Postprocessing

Fig. 3 shows the implementation flow chart for post-processing techniques. All T1-weighted images were preprocessed with the FreeSurfer pipeline (version 7.2.0), freely available software commonly used for brain structural MRI analysis [17,18]. First, T1-weighted images were resliced to a 1-mm isovoxel space with non-uniform intensity normalization. The subsequent automatic reconstruction steps include skull stripping, automatic subcortical segmentation, resampling of the average curvature from the atlas to target, cortical parcellation using the Desikan-Killiany cortical atlas [19], and parcellation statistics

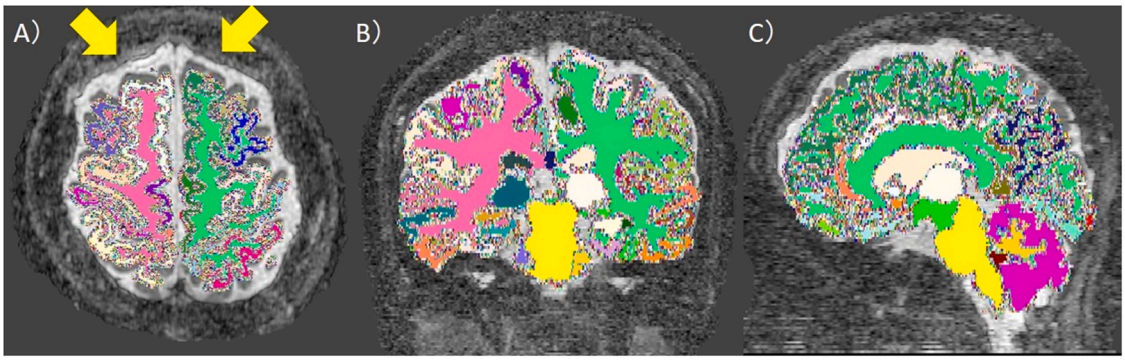

Fig. 4. One excluded ADC map from analyses due to image distortion. Axial (A), coronal (B), and sagittal (C) parcellated T1-weighted images which are overlaid onto corresponding ADC maps. Distortion in the anteroposterior direction is observed.

(https://surfer.nmr.mgh.harvard.edu/fswiki/recon-all). VOI data for bilateral hippocampi, amygdalas, thalami, putamina, caudate nuclei, globi pallidi, nuclei accumbentes, and total corpus callosum were collected from the parcellation atlas. Seventy cortical segments (35 variables in each hemisphere) were also obtained from the atlas. A detailed description of the reconstruction steps has been provided elsewhere [18]. The entire cortex of each subject was visually inspected, and topological defects were manually corrected [20,21]. Mean cortical thicknesses of the right hemisphere, left hemisphere, and 70 cortical thicknesses (35 variables in each hemisphere) were obtained from the Desikan-Killiany atlas.

The acquired Desikan-Killiany atlas of each subject was then resliced with the original T1-weighted images (FOV, 512 ×512 ×150 mm). Subsequently, the resliced segmentation atlas was overlaid onto the corresponding ADC, T1, T2, and PD-maps using ITK-SNAP software (version 3.8.0; https://dss.itksnap.org) [22,23] to compute ADC, T1, T2, and PD. For ADC maps, alignment with the resliced atlas was manually fine-tuned using parallel and/or rotation functions in a rigid manner to improve registration accuracy. After removing VOIs with noise, ADCs, T1s, T2s, and PDs of the supratentorial cortical segments, 5 parts of the corpus callosum (anterior, mid-anterior, central, mid-posterior, and posterior), bilateral cerebral white matter, bilateral cerebellar cortices, bilateral cerebellar white matter, and brainstem were computed, respectively.

2.2. Statistical analysis

Intraclass correlation coefficients (ICCs) were calculated using IBM SPSS® Statistics (Version 28.0.1.1, IBM Corp., Armonk, NY, USA) and graphs were plotted in Prism version 7 (GraphPad Software, La Jolla, San Jose, CA, USA). First, ICCs between test and retest scan with mean cortical thickness of the right hemisphere, left hemisphere, and 70 cortical thicknesses (35 variables in each hemisphere) were evaluated. Second, mean and 95% confidence interval (CI) for ADC, T1, T2, and PD in the supratentorial cortical segments, 5 parts of the corpus callosum, bilateral cerebral white matter, bilateral cerebellar cortex, bilateral cerebellar white matter, and brainstem were calculated. ICCs in ADC, T1, T2, and PD for all parcellated VOI per subject on scan-rescan tests were calculated to assess reproducibility. Based on the 95%CI of the ICC estimate, values of < 0.5, 0.5 to < 0.75, 0.75 to < 0.9, and > 0.9 were taken as indicative of “poor”, “moderate”, “good”, and “excellent” reproducibility, respectively [24]. The Pearson correlation coefficients in ADC, T1, T2, and PD for all parcellated VOI per subject on scan-rescan tests were also assessed. A p-value less than.05 was determined statistically significant.

In addition, Bland-Altman plots in Prism version 7 were used to investigate discrepancies in ADCs, T1s, T2s, and PDs obtained from the two scans, and bias and 95% limits of agreement were calculated.

Table 1
ICCs of cortical thickness, ADC, T1, T2, and PD.

	ICC [95% confidence interval]
R_cortical thickness	0.904[0.83, 0.94]
L_cortical thickness	0.891[0.811, 0.93]
ADC	0.785[0.756, 0.811]
T1	0.986[0.984, 0.988]
T2	0.978[0.97, 0.984]
PD	0.968[0.961, 0.974]

Table 2
Bland-Altman analysis of cortical thickness, ADC, T1, T2, and PD.

	Bias (mean±SD) [95% confidence interval]
R_cortical thickness	-0.06 ± 0.125 [− 0.306, 0.184]
L_cortical thickness	-0.06 ± 0.136 [− 0.331, 0.201]
ADC ($\times 10^{-3}$ mm^2/s)	0.017 ± 0.101 [− 0.215, 0.182]
T1 (ms)	-6.76 ± 46.93 [− 98.74, 85.22]
T2 (ms)	1.01 ± 2.95 [− 4.77, 6.78]
PD (%)	0.34 ± 1.35 [− 2.30, 2.98]

3. Results

All subjects achieved the maximum MMSE score of 30/30, indicating normal cognitive function. Eleven ADC maps and twelve T1, T2, and PD maps were used to analyze test-retest reproducibility. Representative reconstructed ADC, T1, T2, and PD maps are shown in Fig. 3. One ADC map was excluded from analyses due to image distortion (Fig. 4).

3.1. ICCs of right and left cerebral cortical thicknesses (Table 1).

The obtained ICCs for mean cortical thickness of the right and left hemisphere were 0.904 (95%CI, 0.83–0.94) and 0.891 (95%CI, 0.811–0.93), indicating “excellent” and “good” reproducibility, respectively.Table 1.

3.2. Bland-Altman plots of right and left cerebral cortical thickness (Table 2)

The Bland-Altman plot shows right cerebral cortical thickness with bias of − 0.06 ± 0.125 mm (95% limits of agreement, −0.306 to 0.184 mm), and left cerebral cortical thickness with bias of − 0.06 ± 0.136 mm (95% limits of agreement, −0.331 to 0.201 mm).Table 2.

3.3. Mean and 95%CIl of ADC, T1, T2, and PD (Supplemental Table 1–4).

Mean and 95%CI for ADC, T1, T2, and PD in the supratentorial

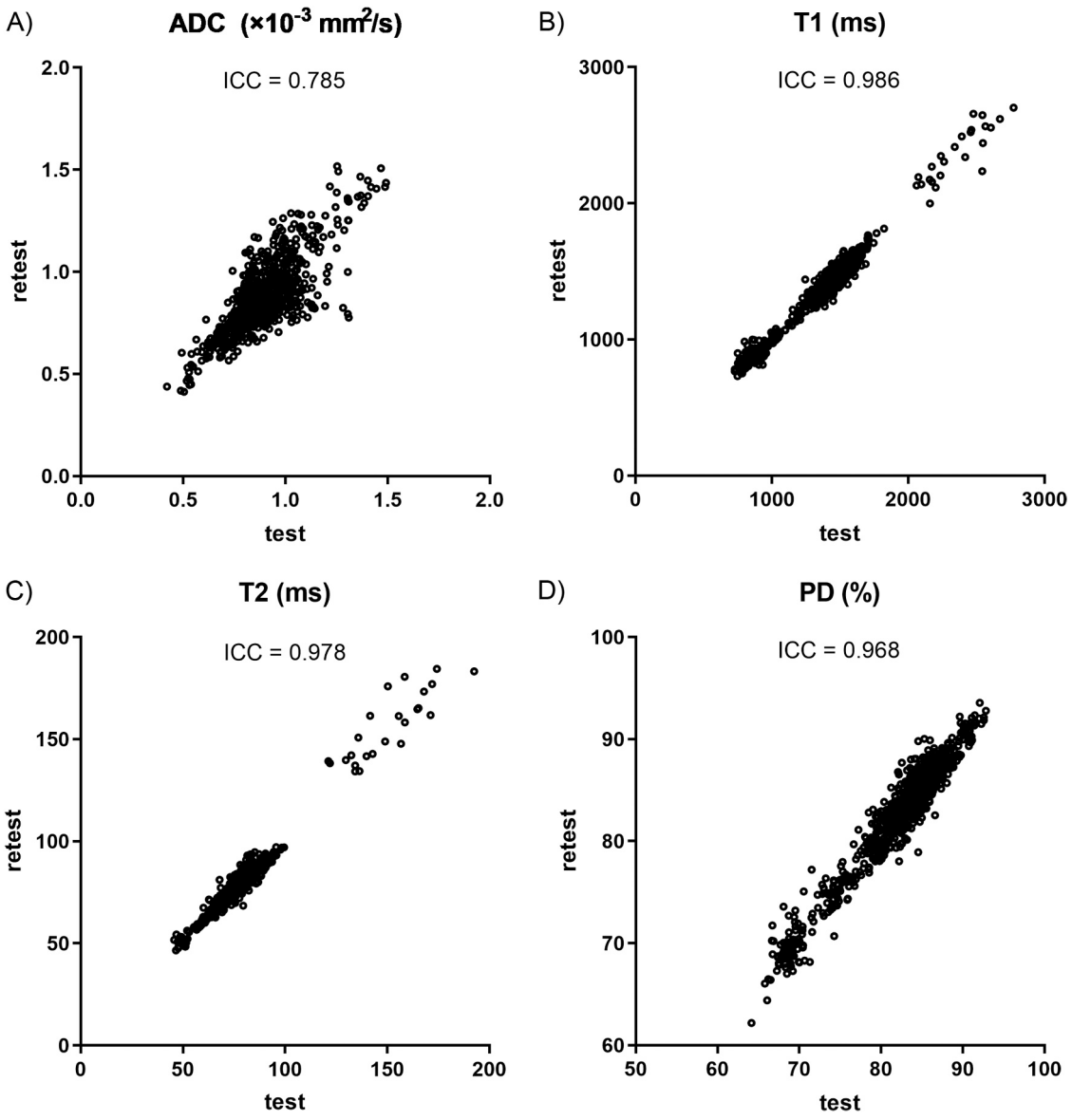

Fig. 5. ICCs of the ADC (A), T1 (B), T2 (C), and PD (D). The ICC for ADC is 0.785 (95%CI 0.756–0.811), indicating "good" reliability. ICCs of T1, T2, and PD are 0.986 (95%CI, 0.984–0.988), 0.978 (95%CI, 0.97–0.984), and 0.968 (95%CI, 0.961–0.974), indicating "excellent" reproducibility.

cortical segments, 5 parts of the corpus callosum, bilateral cerebral white matter, bilateral cerebellar cortex, bilateral cerebellar white matter, and brainstem are shown in Supplemental Table 1. The mean ADC, T1, T2, and PD ranged 0.515–1.408 $\times 10^{-3}$ mm^2/s, 778.9–2532 ms, 50.11–167.5 ms, 68.4–90.86%, respectively. Generally, white matter regions and subcortical nuclei showed low ADC, T1, T2, and PD.

3.4. *ICCs of ADC, T1, T2, and PD (Fig. 5, Table 1).*

The ICC for ADCs was 0.785 (95%CI, 0.756–0.811), indicating "good" reproducibility. The ICCs of T1, T2, and PD were 0.986 (95%CI, 0.984–0.988), 0.978 (95%CI, 0.97–0.984), and 0.968 (95%CI, 0.961–0.974), indicating "excellent" reproducibility.Fig. 5.

3.5. *Pearson correlation coefficients of ADC, T1, T2, and PD*

The Pearson correlation coefficient for ADC, T1, T2, and PD were 0.793, 0.986, 0.981, and 0.970, respectively ($p < 0.001$, each).

3.6. *Bland-Altman analysis of ADC, T1, T2, and PD (Fig. 6, Table 2)*

The Bland-Altman plot shows ADC, T1, T2, and PD with bias of $-0.017 \pm 0.101 \times 10^{-3}$ mm^2/s (95% limits of agreement, −0.215 and 0.182 $\times 10^{-3}$ mm^2/s), -6.76 ± 46.93 ms (95% limits of agreement, −98.74 and 85.22 ms), 1.01 ± 2.95 ms (95% limits of agreement, −4.77 and 6.78 ms), and 0.34 ± 1.35% (95% limits of agreement, −2.30% and 2.98%), respectively.Fig. 6.

4. Discussion

The present study shows high reproducibility of ADC, T1, T2, and PD measurements on the cortex and white matter across the entire brain using pseudo-3D EPICS-DWI and 3D-QALAS with the identical voxel size in healthy adults. These quantitative parameters would provide added value to already available information such as clinical findings, conventional and functional MRI, and positron emission tomography.

The co-registration of ADCs and T1, T2, and PD values with the identical voxel size could characterize the property of brain tissues. First, ADC measurement in the normal human brain has been explored

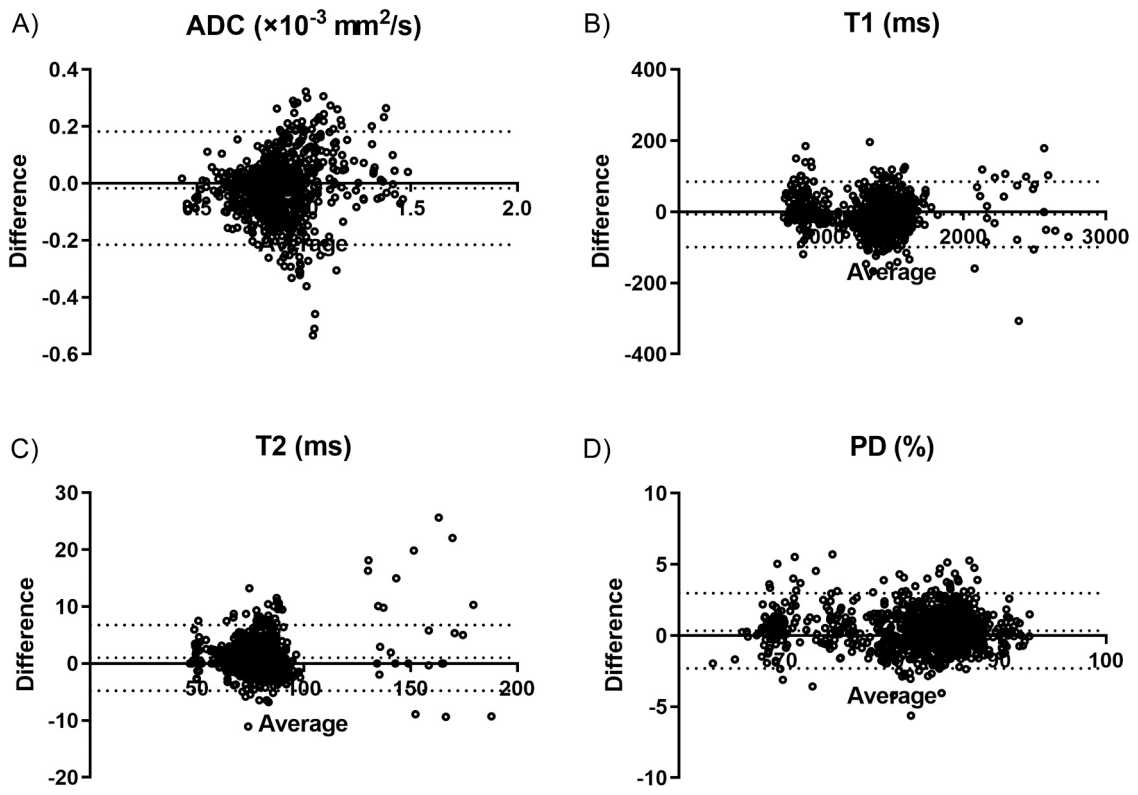

Fig. 6. Bland-Altman plots of the ADCs (A), T1s (B), T2s (C), and PDs (D). The Bland-Altman plot shows ADCs, T1s, T2s, and PDs with bias of − 0.017 ± 0.101 × 10^{-3} mm^2/s, 95% limits of agreement, − 0.215–0.182 × 10^{-3} mm^2/s), − 6.76 ± 46.93 ms (95% limits of agreement, −98.74 to 85.22 ms), 1.01 ± 2.95 ms (95% limits of agreement, −4.77 to 6.78 ms), and 0.34 ± 1.35% (95% limits of agreement, −2.30 to 2.98), respectively.

in detail using 2D DWI with 5-mm thickness by Helenius et al. [25]. ADCs in the white matter and deep grey matter were lower than those of the cerebral cortex in our study. These findings are in line with the literature [25]. Interestingly, ADCs were not influenced by aging [25]. We believe that pseudo-3D EPICS-DWI with high resolution could have applications in the new sequence and ADCs with less partial volume effect may benefit assessment of the biological properties of brain tissues. Then, interactions of water with cholesterol, galactocerebrosides, and proteins of the myelin bilaminar membrane are responsible for the early T1 shortening observed in developing white matter [10]. T1 relaxation time is therefore considered a marker of brain maturation or myelination during brain development [26,27]. In contrast, signal intensities (SIs) on T2-weighted imaging seem much more complicated than those on T1-weighted imaging. Hypointensity on T2-weighted imaging has been indicated to reflect higher myelin content [9,10], while SIs on T2-weighted imaging also change with axonal size, density, coherence, and membrane structure, lipid, protein, and macromolecule content, and water compartmentalization [28]. In central nervous system white matter, free water (> 120 ms), extracellular water (60–90 ms), and myelin water (10–50 ms) all have unique ranges of T2, enabling separation of their relative contribution to overall signal [29,30]. Therefore, T2 relaxation time measurement rather than SIs on T2-weighted imaging would be reasonable to estimate myelin content. The utility of PD values and structural imaging has been well documented with vascular and degenerative diseases [31,32]. We observed the reproducibility of T1, T2, and PD values as well as ADCs with the identical voxel size, indicating that the combination of these parameters provide more information than each parameter alone. Taken together, quantitative parameters of ADC, T1, T2, and PD with identical voxel size would provide added value to already available parameters such as cortical thickness, T1w/T2w, functional MRI, and positron emission tomography. The next step will be to validate our findings by comparing normal subject data to patients with degenerative diseases such as Alzheimer's disease.

The present study has some limitations that merit consideration. First, the present study comprised a small number of cases. Therefore, further validation studies with larger sample size are needed. Second, resliced VOIs at the interface of gray and white matter were allocated as noise, reducing the availability of resliced VOIs for the measurement of ADC, T1, T2, and PD compared to the original VOIs with 1-mm isovoxels. On the other hand, greater information on gray or white matter could be obtained after removing VOIs with noise at the interface of gray and white matter. Lastly, the right insular, right supramarginal and right transverse temporal VOIs could not be distinguished using ITK-SNAP in this study. This might be explained by large numbers of VOIs with noise were allocated when a Desikan-Killiany atlas (with 1-mm isovoxel) was resliced to the original T1-weighted images. To assign appropriate variables was above the capacity of 16-bit integers (between 0 and 65,535) via ITK-SNAP software, and represents another limitation in the present study.

In summary, the combination of EPICS-DWI and 3D-QALAS sequences with identical voxel size could reproducible ADC, T1, T2, and PD measurements for the cortex across the entire brain in healthy adults.

Ethical approval

This study was approved by the institutional review board of our hospital (Kyushu University Institutional Review Board for Clinical Trials). Written informed consent for study participation was obtained from all the study participants.

Funding

This work was supported by the Japan Society for the Promotion of Science (JSPS) KAKENHI Grant number 22K07657, and Research grant from Philips Japan.

CRediT authorship contribution statement

Kikuchi Kazufumi: Writing – review & editing, Visualization. **Wada Tatsuhiro:** Writing – review & editing, Data curation. **Yamashita Koji:** Writing – review & editing, Writing – original draft, Methodology, Investigation, Funding acquisition, Formal analysis, Conceptualization. **Yoneyama Masami:** Writing – review & editing, Writing – original draft, Software. **Mikayama Ryoji:** Writing – review & editing, Data curation. **Murazaki Hiroo:** Writing – review & editing, Data curation. **Watanuki Hiroaki:** Writing – review & editing, Data curation. **Ishigami Kousei:** Writing – review & editing, Supervision. **Togao Osamu:** Writing – review & editing, Supervision, Project administration.

Declaration of Competing Interest

MY: Employee of Philips Japan. KY, KK, TW, HM, HW, RM, KI, and OT: Nothing to disclose.

Appendix A. Supporting information

Supplementary data associated with this article can be found in the online version at doi:10.1016/j.ejro.2023.100516.

References

[1] D. Le Bihan, R. Turner, P. Douek, N. Patronas, Diffusion MR imaging: clinical applications, AJR Am. J. Roentgenol. 159 (1992) 591–599, https://doi.org/10.2214/ajr.159.3.1503032.

[2] T. Yoshiura, F. Mihara, A. Tanaka, T. Noguchi, O. Togao, Y. Kuwabara, H. Honda, Novel method to estimate and display cerebral cortical degeneration using diffusion-weighted magnetic resonance imaging, Magn. Reson Med 54 (2005) 455–459, https://doi.org/10.1002/mrm.20558.

[3] C.J. Wall, E.J. Kendall, A. Obenaus, Rapid alterations in diffusion-weighted images with anatomic correlates in a rodent model of status epilepticus, AJNR Am. J. Neuroradiol. 21 (2000) 1841–1852.

[4] D.K. Jones, S.C. Williams, D. Gasston, M.A. Horsfield, A. Simmons, R. Howard, Isotropic resolution diffusion tensor imaging with whole brain acquisition in a clinically acceptable time, Hum. Brain Mapp. 15 (2002) 216–230, https://doi.org/10.1002/hbm.10018.

[5] M. Yoneyama, K. Morita, J. Peeters, T. Nakaura, M. Van Cauteren, Noise reduction in prostate single-shot DW-EPI utilizing compressed SENSE framework, Proceedings of the 27th annual meeting of ISMRM, Montreal, Canada, 2019 (Abstract 1634).

[6] O. Kamal, S. McTavish, F.N. Harder, A.T. Van, J.M. Peeters, K. Weiss, M. R. Makowski, D.C. Karampinos, R.F. Braren, Noise reduction in diffusion weighted MRI of the pancreas using an L1-regularized iterative SENSE reconstruction, Magn. Reson Imaging 87 (2022) 1–6, https://doi.org/10.1016/j.mri.2021.11.009.

[7] A.T. Vu, E. Auerbach, C. Lenglet, S. Moeller, S.N. Sotiropoulos, S. Jbabdi, J. Andersson, E. Yacoub, K. Ugurbil, High resolution whole brain diffusion imaging at 7T for the Human Connectome Project, Neuroimage 122 (2015) 318–331, https://doi.org/10.1016/j.neuroimage.2015.08.004.

[8] T. Kaga, Y. Noda, T. Mori, N. Kawai, H. Takano, K. Kajita, M. Yoneyama, Y. Akamine, H. Kato, F. Hyodo, M. Matsuo, Diffusion-weighted imaging of the abdomen using echo planar imaging with compressed SENSE: feasibility, image quality, and ADC value evaluation, Eur. J. Radio. 142 (2021), 109889, https://doi.org/10.1016/j.ejrad.2021.109889.

[9] M. Ganzetti, N. Wenderoth, D. Mantini, Whole brain myelin mapping using T1- and T2-weighted MR imaging data, Front Hum. Neurosci. 8 (2014) 671, https://doi.org/10.3389/fnhum.2014.00671.

[10] A.J. Barkovich, Concepts of myelin and myelination in neuroradiology, AJNR Am. J. Neuroradiol. 21 (2000) 1099–1109.

[11] M.F. Glasser, D.C. Van Essen, Mapping human cortical areas in vivo based on myelin content as revealed by T1- and T2-weighted MRI, J. Neurosci. 31 (2011) 11597–11616, https://doi.org/10.1523/JNEUROSCI.2180-11.2011.

[12] S. Nerland, K.N. Jorgensen, W. Nordhoy, I.I. Maximov, R.A.B. Bugge, L.T. Westlye, O.A. Andreassen, O.M. Geier, I. Agartz, Multisite reproducibility and test-retest reliability of the T1w/T2w-ratio: a comparison of processing methods, Neuroimage 245 (2021), 118709, https://doi.org/10.1016/j.neuroimage.2021.118709.

[13] A. Hagiwara, M. Hori, K. Kamagata, M. Warntjes, D. Matsuyoshi, M. Nakazawa, R. Ueda, C. Andica, S. Koshino, T. Maekawa, R. Irie, T. Takamura, K.K. Kumamaru, O. Abe, S. Aoki, Myelin measurement: comparison between simultaneous tissue relaxometry, magnetization transfer saturation index, and T1w/T2w ratio methods, Sci. Rep. 8 (2018) 10554, https://doi.org/10.1038/s41598-018-28852-6.

[14] S. Kvernby, M.J. Warntjes, H. Haraldsson, C.J. Carlhall, J. Engvall, T. Ebbers, Simultaneous three-dimensional myocardial T1 and T2 mapping in one breath hold with 3D-QALAS, J. Cardiovasc Magn. Reson 16 (2014) 102, https://doi.org/10.1186/s12968-014-0102-0.

[15] S. Fujita, A. Hagiwara, M. Hori, M. Warntjes, K. Kamagata, I. Fukunaga, M. Goto, H. Takuya, K. Takasu, C. Andica, T. Maekawa, M.Y. Takemura, R. Irie, A. Wada, M. Suzuki, S. Aoki, 3D quantitative synthetic MRI-derived cortical thickness and subcortical brain volumes: Scan-rescan repeatability and comparison with conventional T1 -weighted images, J. Magn. Reson Imaging 50 (2019) 1834–1842, https://doi.org/10.1002/jmri.26744.

[16] S. Fujita, A. Hagiwara, M. Hori, M. Warntjes, K. Kamagata, I. Fukunaga, C. Andica, T. Maekawa, R. Irie, M.Y. Takemura, K.K. Kumamaru, A. Wada, M. Suzuki, Y. Ozaki, O. Abe, S. Aoki, Three-dimensional high-resolution simultaneous quantitative mapping of the whole brain with 3D-QALAS: An accuracy and repeatability study, Magn. Reson Imaging 63 (2019) 235–243, https://doi.org/10.1016/j.mri.2019.08.031.

[17] B. Fischl, D.H. Salat, E. Busa, M. Albert, M. Dieterich, C. Haselgrove, A. van der Kouwe, R. Killiany, D. Kennedy, S. Klaveness, A. Montillo, N. Makris, B. Rosen, A. M. Dale, Whole brain segmentation: automated labeling of neuroanatomical structures in the human brain, Neuron 33 (2002) 341–355, https://doi.org/10.1016/s0896-6273(02)00569-x.

[18] B. Fischl, FreeSurfer, Neuroimage 62 (2012) 774–781, https://doi.org/10.1016/j.neuroimage.2012.01.021.

[19] R.S. Desikan, F. Segonne, B. Fischl, B.T. Quinn, B.C. Dickerson, D. Blacker, R. L. Buckner, A.M. Dale, R.P. Maguire, B.T. Hyman, M.S. Albert, R.J. Killiany, An automated labeling system for subdividing the human cerebral cortex on MRI scans into gyral based regions of interest, Neuroimage 31 (2006) 968–980, https://doi.org/10.1016/j.neuroimage.2006.01.021.

[20] Y. Otsuka, S. Kakeda, K. Sugimoto, A. Katsuki, L.H. Nguyen, R. Igata, K. Watanabe, I. Ueda, T. Kishi, N. Iwata, Y. Korogi, R. Yoshimura, COMT polymorphism regulates the hippocampal subfield volumes in first-episode, drug-naive patients with major depressive disorder, Neuropsychiatr. Dis. Treat. 15 (2019) 1537–1545, https://doi.org/10.2147/NDT.S199598.

[21] K. Yamashita, T. Kuwashiro, K. Ishikawa, K. Furuya, S. Harada, S. Shin, N. Wada, C. Hirakawa, Y. Okada, T. Noguchi, Right entorhinal cortical thickness is associated with Mini-Mental State Examination scores from multi-country datasets using MRI, Neuroradiology 64 (2022) 279–288, https://doi.org/10.1007/s00234-021-02767-y.

[22] P.A. Yushkevich, J. Piven, H.C. Hazlett, R.G. Smith, S. Ho, J.C. Gee, G. Gerig, User-guided 3D active contour segmentation of anatomical structures: significantly improved efficiency and reliability, Neuroimage 31 (2006) 1116–1128, https://doi.org/10.1016/j.neuroimage.2006.01.015.

[23] P.A. Yushkevich, J.B. Pluta, H. Wang, L. Xie, S.L. Ding, E.C. Gertje, L. Mancuso, D. Kliot, S.R. Das, D.A. Wolk, Automated volumetry and regional thickness analysis of hippocampal subfields and medial temporal cortical structures in mild cognitive impairment, Hum. Brain Mapp. 36 (2015) 258–287, https://doi.org/10.1002/hbm.22627.

[24] T.K. Koo, M.Y. Li, A guideline of selecting and reporting intraclass correlation coefficients for reliability research, J. Chiropr. Med 15 (2016) 155–163, https://doi.org/10.1016/j.jcm.2016.02.012.

[25] J. Helenius, L. Soinne, J. Perkio, O. Salonen, A. Kangasmaki, M. Kaste, R.A. Carano, H.J. Aronen, T. Tatlisumak, Diffusion-weighted MR imaging in normal human brains in various age groups, AJNR Am. J. Neuroradiol. 23 (2002) 194–199.

[26] A.J. Barkovich, B.O. Kjos, D.E. Jackson Jr., D. Norman, Normal maturation of the neonatal and infant brain: MR imaging at 1.5 T, Radiology 166 (1988) 173–180, https://doi.org/10.1148/radiology.166.1.3336675.

[27] S. Eminian, S.D. Hajdu, R.A. Meuli, P. Maeder, P. Hagmann, Rapid high resolution T1 mapping as a marker of brain development: normative ranges in key regions of interest, PLoS One 13 (2018), e0198250, https://doi.org/10.1371/journal.pone.0198250.

[28] S.C. Deoni, E. Mercure, A. Blasi, D. Gasston, A. Thomson, M. Johnson, S. C. Williams, D.G. Murphy, Mapping infant brain myelination with magnetic resonance imaging, J. Neurosci. 31 (2011) 784–791, https://doi.org/10.1523/JNEUROSCI.2106-10.2011.

[29] W.A. Stewart, A.L. MacKay, K.P. Whittall, G.R. Moore, D.W. Paty, Spin-spin relaxation in experimental allergic encephalomyelitis. Analysis of CPMG data using a non-linear least squares method and linear inverse theory, Magn. Reson Med 29 (1993) 767–775, https://doi.org/10.1002/mrm.1910290608.

[30] F. Heath, S.A. Hurley, H. Johansen-Berg, C. Sampaio-Baptista, Advances in noninvasive myelin imaging, Dev. Neurobiol. 78 (2018) 136–151, https://doi.org/10.1002/dneu.22552.

[31] D. Mungas, W.J. Jagust, B.R. Reed, J.H. Kramer, M.W. Weiner, N. Schuff, D. Norman, W.J. Mack, L. Willis, H.C. Chui, MRI predictors of cognition in subcortical ischemic vascular disease and Alzheimer's disease, Neurology 57 (2001) 2229–2235, https://doi.org/10.1212/wnl.57.12.2229.

[32] A.M. Brickman, G. Tosto, J. Gutierrez, H. Andrews, Y. Gu, A. Narkhede, B. Rizvi, V. Guzman, J.J. Manly, J.P. Vonsattel, N. Schupf, R. Mayeux, An MRI measure of degenerative and cerebrovascular pathology in Alzheimer disease, Neurology 91 (2018) e1402–e1412, https://doi.org/10.1212/WNL.0000000000006310.